Submitted to ApJL.

The Spectrum of the Mass Donor Star in SS 433

D. R. Gies[1], W. Huang[1], and M. V. McSwain

Center for High Angular Resolution Astronomy, Department of Physics and Astronomy
Georgia State University, Atlanta, GA 30303
Electronic mail: gies@chara.gsu.edu, huang@chara.gsu.edu, mcswain@chara.gsu.edu

ABSTRACT

We present results from a short series of blue, moderate resolution spectra of the microquasar binary, SS 433. The observations were made at a time optimized to find the spectrum of the donor star, i.e., when the donor was in the foreground and well above the plane of the obscuring disk. In addition to the well-known stationary and jet emission lines, we find evidence of a weak absorption spectrum that resembles that of an A-type evolved star. These lines display radial velocity shifts opposite to those associated with the disk surrounding the compact star, and they appear strongest when the disk is maximally eclipsed. All these properties suggest that these absorption lines form in the atmosphere of the hitherto unseen mass donor star in SS 433. The radial velocity shifts observed are consistent with a mass ratio $M_X/M_O = 0.57 \pm 0.11$ and masses of $M_O = (19 \pm 7)\ M_\odot$ and $M_X = (11 \pm 5)\ M_\odot$. These results indicate that the system consists of an evolved, massive donor and a black hole mass gainer.

Subject headings: stars: early-type — stars: individual (SS 433; V1343 Aql) — X-rays: binaries

1. Introduction

SS 433 is still one of the most mysterious of the X-ray binaries even after some 25 years of observation (Margon 1984; Zwitter et al. 1989; Gies et al. 2002). We know that the mass donor feeds an enlarged accretion disk surrounding a neutron star or black hole companion,

[1]Visiting Astronomer, University of Texas McDonald Observatory.

and a small portion of this inflow is ejected into relativistic jets that are observed in optical and X-ray emission lines and in high resolution radio maps. There are two basic timescales that control the spectral appearance and system dynamics, a 162 d disk and jet precessional cycle and a 13 d orbital period. The mass function derived from the He II λ4686 emission line indicates that the donor star mass is in excess of 8 $M_{\odot}$ (Fabrika & Bychkova 1990), and the donor is probably a Roche-filling, evolved star (King et al. 2000). However, the spectral signature of this star has eluded detection. This is probably because the binary is embedded in an expanding thick disk that is fed by the wind from the super-Eddington accretion disk (Zwitter et al. 1991). The outer regions of this equatorial thick disk have been detected in high resolution radio measurements by Paragi et al. (1999) and Blundell et al. (2001). We recently showed how many of the properties of the "stationary" emission lines can be explained in terms of a disk wind (Gies et al. 2002).

The task of finding the spectrum of the donor is crucial because without a measurement of its orbital motion, the mass of the relativistic star is unknown. The best opportunity to observe the flux from the donor occurs at the precessional phase when the disk normal is closest to our line of sight and the donor star appears well above the disk plane near the donor inferior conjunction orbital phase (Gies et al. 2002). This configuration occurs only a few nights each year for ground-based observers. The choice of spectral region is also important. Goranskii et al. (1998a) found that the regular eclipse and precessional variations seen clearly in the blue are lost in the red due to an erratically variable flux component. Thus, we need to search for the donor spectrum blueward of the R-band in order to avoid this variable component. On the other hand, the color variations observed during eclipses suggest that the donor is cooler than the central portions of the disk (Antokhina & Cherepashchuk 1987; Goranskii et al. 1997). Thus, the disk will tend to contribute a greater fraction of the total flux at lower wavelengths. The best compromise is in the blue where there are a number of strong absorption lines in B- and later-type stars.

Here we present the results of a blue spectral search for the donor's spectrum made during an optimal disk and orbital configuration in 2002 June (§2). We first discuss the dominant emission features formed in the jets and disk wind (§3). We then focus on a much weaker set of absorption lines (§4), and we present arguments linking these to the photosphere of the donor star.

2. Observations

The blue spectra of SS 433 were obtained on three consecutive nights, 2002 June 5 – 7, with the Large Cassegrain Spectrograph (LCS) on the 2.7-m Harlan J. Smith Telescope at

the University of Texas McDonald Observatory (Cochran 2002). These dates correspond to precessional phases between $\Psi = 0.998$ and 0.011 (where $\Psi = 0.0$ corresponds to the time when the jets are closest to our line of sight and their emission lines attain their extremum radial velocities) and to orbital phases between $\phi = 0.012$ and 0.178 (where mid-eclipse and donor inferior conjunction occur at $\phi = 0.0$) according to the phase relations adopted in Gies et al. (2002). The spectra were made in first order with the #46 grating (1200 grooves mm^{-1}, blazed at 4000 Å), and they cover the wavelength range between 4060 and 4750 Å. We used a long slit configuration with a slit width of $2\farcs0$, which corresponds to a projected width of 2 pixels FWHM on the detector, a 800×800 format TI CCD with 15μm square pixels. The reciprocal dispersion is 0.889 Å pixel^{-1} and the spectral resolving power is $\lambda/\triangle\lambda = 2500$. Unfortunately, the weather was partially cloudy throughout the run, and we were only able to obtain a few consecutive, 20 minute exposures on each night. We also obtained a full suite of calibration bias, dome flat field, and argon comparison frames throughout the run.

The spectra were extracted and calibrated using standard routines in IRAF[2]. We co-added all the consecutive spectra from a given night to increase the signal-to-noise ratio (S/N). The co-added spectra were then rectified to a unit continuum by the fitting of line-free regions. Note that this rectification process arbitrarily removes the continuum flux variations that occurred in SS 433 during the eclipse. All the spectra were then transformed to a common heliocentric wavelength grid for ease of comparison. The final S/N ratios in the continuum at the long-wavelength end of the spectra are 31, 16, and 40 pixel^{-1} for the three consecutive nights, respectively.

3. Emission Line Spectrum

Our three spectra are shown in chronological sequence in Figure 1. This part of the spectrum is dominated by the familiar strong emission lines of Hδ, Hγ, and He II λ4686 (Murdin et al. 1980; Panferov & Fabrika 1997; Fabrika et al. 1997a). Most of these lines appear stronger in the first, mid-eclipse spectrum made when the continuum flux was low. We begin by examining the radial velocity and intensity variations of the emission lines before turning to the weaker absorption features in the next section.

The only strong jet emission feature in this spectral range at this time is the blueshifted H$\beta-$ line (formed in the approaching jet), which is found just longward of Hγ. This spectral

[2]IRAF is distributed by the National Optical Astronomy Observatories, which is operated by the Association of Universities for Research in Astronomy, Inc., under cooperative agreement with the National Science Foundation.

range should also contain redshifted jet components from the upper Balmer sequence (from the Balmer limit at ≈ 4267 Å to Hϵ at ≈ 4645 Å), but, if present, they are too weak to detect in our spectra. We measured the radial velocity of the H$\beta-$ emission feature by fitting a single Gaussian in each case. These measurements are partially compromised by the appearance of multiple sub-peaks in some cases (see the final profile that contains a redshifted, sub-peak corresponding in radial velocity to the "bullet" that appeared on the previous night) and by the possible existence of very weak He I λ4387 emission. Nevertheless, these measurements show the familiar oscillations in the jet velocities due to the tidal "nodding" of the accretion disk (Vermeulen et al. 1993; Gies et al. 2002). Table 1 lists the heliocentric Julian date for the mid-time of each observation, the observed H$\beta-$ radial velocity as $z = V_r/c$ (estimated errors ± 0.001), and the predicted z value based upon the extrapolation of the fit to the Hα jet velocities observed between 1998 and 1999 (Gies et al. 2002). The good agreement between the observed and predicted motions suggests that our jet precessional velocity fit is still reliable 3 years after the last Hα observations.

The stationary emission lines generally fall into two categories: lines like He II λ4686 that form in a region symmetric about the center of the accretion disk and that show orbital radial velocity curves of the form $-K_1 \sin(2\pi\phi) + V_1$, and features like the hydrogen Balmer lines that probably form in a large volume in the disk's wind and have a radial velocity variation of the form $K_2 \cos(2\pi\phi) + V_2$ (Gies et al. 2002). We measured the radial velocities of the stationary lines in our spectra to confirm their radial velocity behavior. The profiles were obtained by Gaussian fitting in all cases except for the N III + C III complex near 4644 Å, where we measured relative shifts by cross-correlating the profiles for the second and third nights against that from the first night. Our results are listed in Table 2 (errors are ± 30 km s^{-1}). All the lines showed the blueward motion expected in this phase interval, but with a larger amplitude than predicted. The largest decline was found in N III + C III and He II λ4686, which decreased in radial velocity by ≈ 214 km s^{-1} over the duration of observations. Fabrika & Bychkova (1990) estimate that the disk semiamplitude is $K_1 \approx 175$ km s^{-1}, much smaller than we observed. The same situation occurred in lines of the other group, Hδ, Hγ, and He I λ4471 which declined by some 108 km s^{-1} (compared to the expected $K_2 \approx 64$ km s^{-1}; Gies et al. (2002)). We speculate that this difference is due to the emergence of the approaching portion of the disk after the eclipse, which biases the radial velocities to more negative values.

The other clue about the origin of the stationary lines comes from their intensity variations during the eclipse. If the emission source has a constant flux, then during eclipse the line will appear proportionally stronger relative to the lower continuum flux. However, if the emission source is also (partially) eclipsed, then the relative strength in rectified intensity remains approximately constant in eclipse. We show in Table 3 the rectified intensities of

the emission lines for the first two nights relative to that on the final night. The final column gives the predicted constant emission flux variation relative to the last night based upon the V-band light curve (Goranskii et al. (1998b); see their Fig. 7b) and the $B - V$ color variations (Goranskii et al. (1997); see their Fig. 3). We find that most of the line intensities decreased by a factor of 2.4× between the first (mid-eclipse) and last (out-of-eclipse) observations, compared to an expected decrease of 1.9× for a constant emission flux source. This difference is probably not significant since the intrinsic system flux does vary on short timescales, but the result does suggest that most of the lines form in regions large compared to the continuum-forming part of the accretion disk (so that the continuum-forming inner disk is eclipsed while the much larger line forming region suffers only minor occultation). The main exception is the N III + C III line which varies little in rectified intensity and must therefore form co-spatially with the continuum in the inner, hot part of the accretion disk. The other possible exception is the He II λ4686 line. Goranskii et al. (1997) and Fabrika et al. (1997b) observed profile shape variations during the eclipse that we also find (for example, from single- to double-peaked with egress from the eclipse), and they argue that the feature has two components, one formed in gas close to the disk center (eclipsed) and one formed in a larger volume (not eclipsed). This assessment agrees with the fact that, after the N III + C III line, the He II λ4686 feature shows the second smallest decrease in rectified flux, suggesting that its line forming region is more occulted during the eclipse than is the case for the H and He I lines (formed in the larger disk wind).

4. Absorption Line Spectrum

We were struck in comparing the individual spectra by the similarity of patterns of what might first be considered "noise" in the continuum between the strong emission lines. We formed a global average spectrum with each spectrum weighted by the square of its S/N ratio, and an expanded version of this average spectrum is shown in Figures 2 and 3. We show below the average SS 433 plot examples of stellar spectra that could correspond to the spectral type of the donor star. The two B-star spectra were obtained from the atlas of Walborn & Fitzpatrick (1990), and we obtained the spectrum of the A-supergiant, HD 148743, with the LCS. All these spectra were Gaussian smoothed to an effective 2 pixel resolution of 1.78 Å FWHM in order to compare them at the same instrumental resolution. We see that there is a significant (and largely unresolved) system of absorption lines in SS 433 that has eluded detection in earlier work. The line patterns bear little resemblance to those in B-supergiants but there are a number of features in common with the A-supergiant ($T_{\rm eff}$ = 7800 K; Venn (1995)). We show some preliminary identifications of the absorption lines based upon lists in Ballereau (1980) and Venn (1995).

We measured the radial velocity of the absorption system by cross-correlating subsections of the spectrum containing the deepest features with the same in the first spectrum of the set. These relative velocities are listed in the final column of Table 2. (We found that the absorption lines in the first spectrum had a cross-correlation velocity of -39 ± 20 km s^{-1} compared to the rest frame spectrum of HD 148743, so adding this value to the velocities in Table 2 gives an estimate of the absolute velocities.) Unlike the emission lines, the absorption lines moved significantly redward during the run, as expected for the donor star.

Direct inspection of Figure 1 suggests that the absorption line spectrum grew fainter with egress from the eclipse, as predicted for the donor's spectrum. It is difficult to measure the change in individual lines, so we measured the strength of the cross-correlation of the absorption lines with those in HD 148743. The relative cross-correlation intensities are listed in the second last column of Table 3 (errors of ± 0.5). The absorption depths weakened in the same way as the emission intensities, suggesting that both became diluted by the emerging flux of the disk.

Both the radial velocity and intensity variations indicate that the absorption lines form in the long-sought donor star. If they were formed in the interstellar medium (the case of the absorptions at 4428, 4501, and 4726 Å), then we would observe no velocity or intensity variations through these eclipse phases. Similar arguments rule out formation in an extended "shell" surrounding the binary system.

The absorption line velocities are insufficient for a general orbital solution, but we can make a restricted solution if we assume that the orbit is circular and we adopt the orbital period and epoch of mid-eclipse from Goranskii et al. (1998b). Then we can solve for two parameters, the systemic velocity, V_0, and orbital semiamplitude, K_O, from our 3 radial velocity measurements of the optical star. We used the orbital fitting code of Morbey & Brosterhus (1974) to find $V_0 = (-44 \pm 9)$ km s^{-1} and $K_O = (100 \pm 15)$ km s^{-1} with residual errors of 9 km s^{-1}. Fabrika & Bychkova (1990) find the semi-amplitude of the disk is $K_X = (175 \pm 20)$ km s^{-1} based upon the He II λ4686 radial velocity curve. They adopt the system inclination from the "kinematical" model of the jets to arrive at a mass relation, $M_O/(1+q)^2 = (7.7 \pm 2.7)\ M_\odot$ where the mass ratio is $q = M_X/M_O$. We can now combine the semiamplitudes to estimate the mass ratio, $q = K_O/K_X = 0.57 \pm 0.11$, and the resulting masses are $M_O = (19 \pm 7)\ M_\odot$ and $M_X = (11 \pm 5)\ M_\odot$. Thus, our results suggest that the companion is a black hole.

The absorption line depths strengthen from main sequence to supergiant in the A stars, and they appear sufficiently strong in the first eclipse spectrum to rule out a main sequence class. The donor star probably fills the critical Roche surface, and our estimate of the mass

ratio indicates a Roche volume radius of $(31 \pm 3)\ R_\odot$, consistent with a supergiant class. Thus, our results for SS 433 support the evolutionary scenario described by King et al. (2000) in which mass transfer is occurring on a thermal timescale as the donor crosses the Hertzsprung gap.

We can estimate the magnitude difference between the star and disk, $\triangle B$, based upon the apparent line depths. Suppose that during the central eclipse a disk flux of F_1 is occulted while a disk flux of F_2 and donor star flux $F_\star$ remain visible. The stellar line depths will then appear diluted by a factor $F_\star/(F_2 + F_\star)$. The observed line depths during eclipse (relative to the spectrum of the A-supergiant) suggest that the dilution is minimal, so $F_2/F_\star = 0$ to 1. Based upon the line intensity variations we observed (Table 3), the ratio of out-of-eclipse to mid-eclipse flux is 2.38 ± 0.15, and thus, the disk to star flux ratio is $(F_1 + F_2)/F_\star = 1.4$ to 2.8 (or $\triangle B = 0.3$ to 1.4 mag). A donor star this bright may appear to be in conflict with earlier results (Antokhina & Cherepashchuk 1987; Gies et al. 2002), but we suspect that the star is heavily obscured at other precessional and orbital phases so that the line spectrum is difficult to find (and thus the estimate of the donor star's flux based on the absence of the lines will to be too low).

Clearly our results should be regarded as preliminary since we have only observed the absorption spectrum during this one eclipse event, and SS 433 is known to display spectroscopic variations on timescales unrelated to the orbit. Nevertheless, confirmation of our results (especially in spectra of higher S/N and resolution) would be of particular importance in determining the stellar parameters of the donor ($T_{\rm eff}$, $\log g$, and abundance) and in refining the mass estimates. We emphasize again that the successful detection of the donor spectrum is probably limited to times near $\Psi = 0$ and $\phi = 0$. The next opportunities will occur near 2003 April 28 and 2003 October 2.

We are grateful to the staff of McDonald Observatory and especially Dr. Anita Cochran for their help. Support for this work was provided by NASA through grant number GO-8308 from the Space Telescope Science Institute, which is operated by the Association of Universities for Research in Astronomy, Inc., under NASA contract NAS5-26555. Institutional support has been provided from the GSU College of Arts and Sciences and from the Research Program Enhancement fund of the Board of Regents of the University System of Georgia, administered through the GSU Office of the Vice President for Research. We gratefully acknowledge all this support.

REFERENCES

Antokhina, E. A., & Cherepashchuk, A. M. 1987, Soviet Astr., 31, 295

Ballereau, D. 1980, A&AS, 41, 305

Blundell, K. M., Mioduszewski, A., Muxlow, T. W. B., Podsiadlowski, P., & Rupen, M. 2001, ApJ, 562, L79

Cochran, A. L. 2002, User's Manual for the Large Cassegrain Spectrograph and Automated Telescope Offset Guider (Austin: Univ. of Texas McDonald Obs.) (http://www.as.utexas.edu/mcdonald/computer/atog_manual.pdf)

Fabrika, S. N., & Bychkova, L. V. 1990, A&A, 240, L5

Fabrika, S. N., Panferov, A. A., Bychkova, L. V., & Rakhimov, V. Yu. 1997b, Bull. Special Astrophys. Obs., 43, 95

Fabrika, S. N., et al. 1997a, Bull. Special Astrophys. Obs., 43, 109

Gies, D. R., McSwain, M. V., Riddle, R. L., Wang, Z., Wiita, P. J., & Wingert, D. W. 2002, ApJ, 566, 1069

Goranskii, V. P., Fabrika, S. N., Rakhimov, V. Yu., Panferov, A. A., Belov, A. N., & Bychkova, L. V. 1997, Astr. Rep., 41, 656

Goranskii, V. P., Esipov, V. F., & Cherepashchuk, A. M. 1998a, Astr. Rep., 42, 336

Goranskii, V. P., Esipov, V. F., & Cherepashchuk, A. M. 1998b, Astr. Rep., 42, 209

King, A. R., Taam, R. E., & Begelman, M. C. 2000, ApJ, 530, L25

Margon, B. 1984, ARA&A, 22, 507

Morbey, C. L., & Brosterhus, E. B. 1974, PASP, 86, 455

Murdin, P., Clark, D. H., & Martin, P. G. 1980, MNRAS, 193, 135

Panferov, A. A., & Fabrika, S. N. 1997, Astr. Rep, 41, 506

Paragi, Z., Vermeulen, R. C., Fejes, I., Schilizzi, R. T., Spencer, R. E., & Stirling, A. M. 1999, A&A, 348, 910

Venn, K. A. 1995, ApJS, 99, 659

Vermeulen, R. C., et al. 1993, A&A, 270, 204

Walborn, N. R., & Fitzpatrick, E. L. 1990, PASP, 102, 379

Zwitter, T., Calvani, M., Bodo, G., & Massaglia, S. 1989, Fund. Cosmic Phys., 13, 309

Zwitter, T., Calvani, & D'Odorico, S. 1991, A&A, 251, 92

AAS LaTeX macros v5.0.

Fig. 1.— The rectified spectra of SS 433 marked with labels for the prominent features. The spectra are shown chronologically from the first night (*upper*) to the last night (*lower*), and the spectrum for each night is offset by unity for clarity. The orbital phases of observation, ϕ, are listed above each spectrum.

Fig. 2.— A detailed plot of the low wavelength portion of the co-added spectrum of SS 433 (*thick line*). The individual spectra were shifted to the rest frame prior to co-addition. Several examples of the predicted donor spectrum are shown below (*thin lines*): HD 148743 (A7 Ib), β Ori (B8 Ia), and HD 148688 (B1 Ia). All the spectral intensities were increased by a factor of 2 and offset in intensity for ease of comparison. Preliminary identifications are given for a number of weak absorption lines in the spectrum of SS 433. A plus sign following the identification indicates a blend of multiple lines.

Fig. 3.— A detailed plot of the long wavelength portion of the co-added spectrum of SS 433 in the same format as Fig. 2.

Table 1. Jet Radial Velocity Measurements

Date (HJD - 2450000)	Observed $z(\mathrm{H}\beta-)$	Predicted $z(\mathrm{H}\alpha-)$
2430.7616	−0.099	−0.098
2431.8226	−0.097	−0.095
2432.9381	−0.103	−0.100

Table 2. Stationary Line Radial Velocity Measurements

Date (HJD - 2450000)	V_r(Hδ) (km s^{-1})	V_r(Hγ) (km s^{-1})	V_r(He I) (km s^{-1})	V_r(N III)[a] (km s^{-1})	V_r(He II) (km s^{-1})	V_r(Abs.)[a] (km s^{-1})
2430.7616	169	204	264	0	168	0
2431.8226	25	118	204	-96	50	38 ± 35
2432.9381	77	80	157	-216	-44	87 ± 15

[a]Cross-correlation velocity relative to first observation.

Table 3. Relative Line Intensities F_l/F_c : $F_l/F_c(\phi = 0.178)$

Orbital Phase	Hδ	Hγ	He I	N III	He II	H$\beta-$	Abs.[a]	B Light Curve[b]
0.012.....	2.28	2.53	2.47	1.20	2.16	2.44	2.6	1.91
0.093.....	1.58	1.38	1.56	1.16	1.40	1.25	1.5	1.22

[a]Cross-correlation intensity relative to that at phase 0.178.

[b]Prediction for constant F_l relative to phase 0.178.

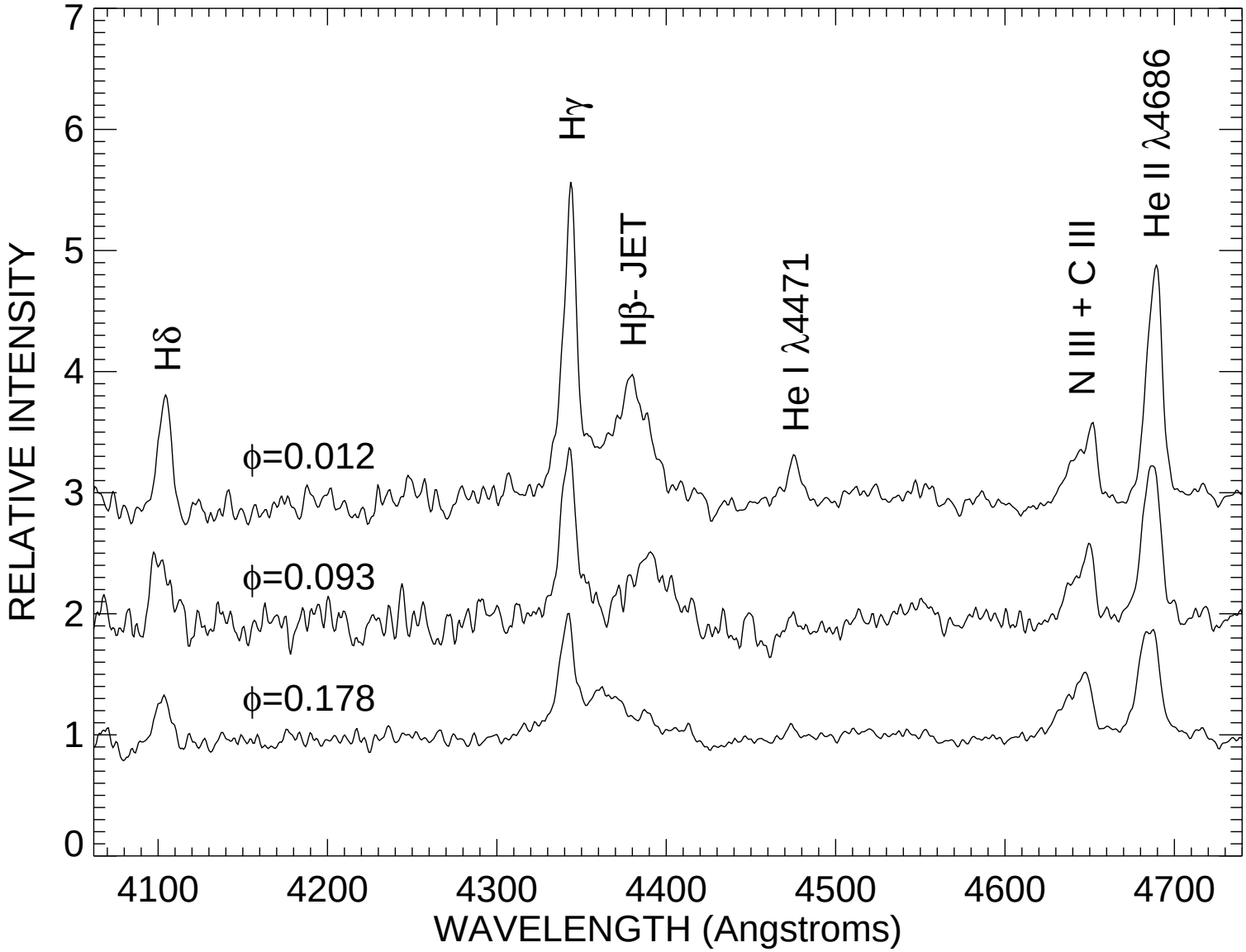
RELATIVE INTENSITY
WAVELENGTH (Angstroms)
Hδ
Hγ
Hβ- JET
He I λ4471
N III + C III
He II λ4686
ϕ=0.012
ϕ=0.093
ϕ=0.178
0
1
2
3
4
5
6
7
4100
4200
4300
4400
4500
4600
4700

Fig. 1.—

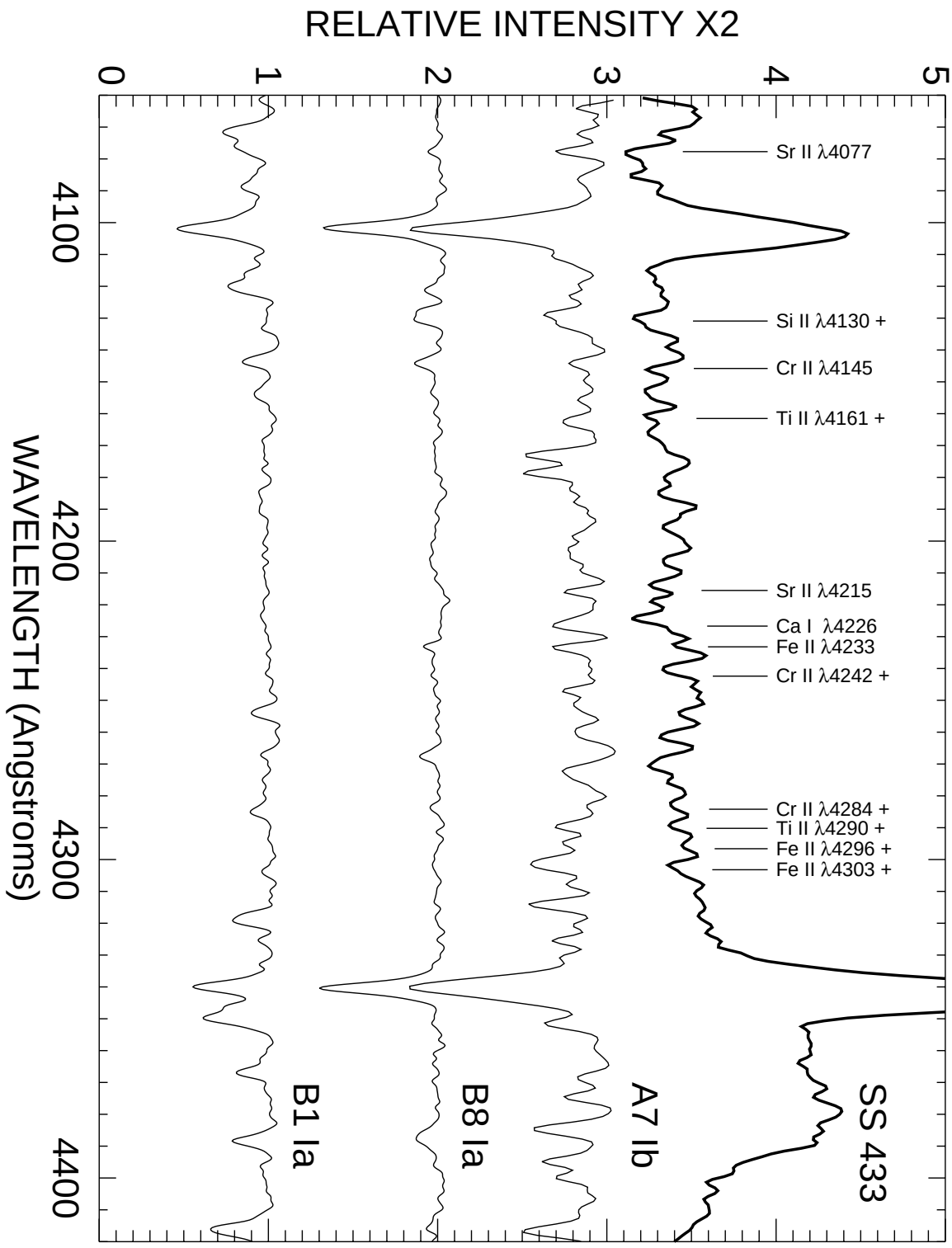
RELATIVE INTENSITY X2
0
1
2
3
4
5
4100
4200
4300
4400
WAVELENGTH (Angstroms)
Sr II λ4077
Si II λ4130 +
Cr II λ4145
Ti II λ4161 +
Sr II λ4215
Ca I λ4226
Fe II λ4233
Cr II λ4242 +
Cr II λ4284 +
Ti II λ4290 +
Fe II λ4296 +
Fe II λ4303 +
B1 Ia
B8 Ia
A7 Ib
SS 433

Fig. 2.—

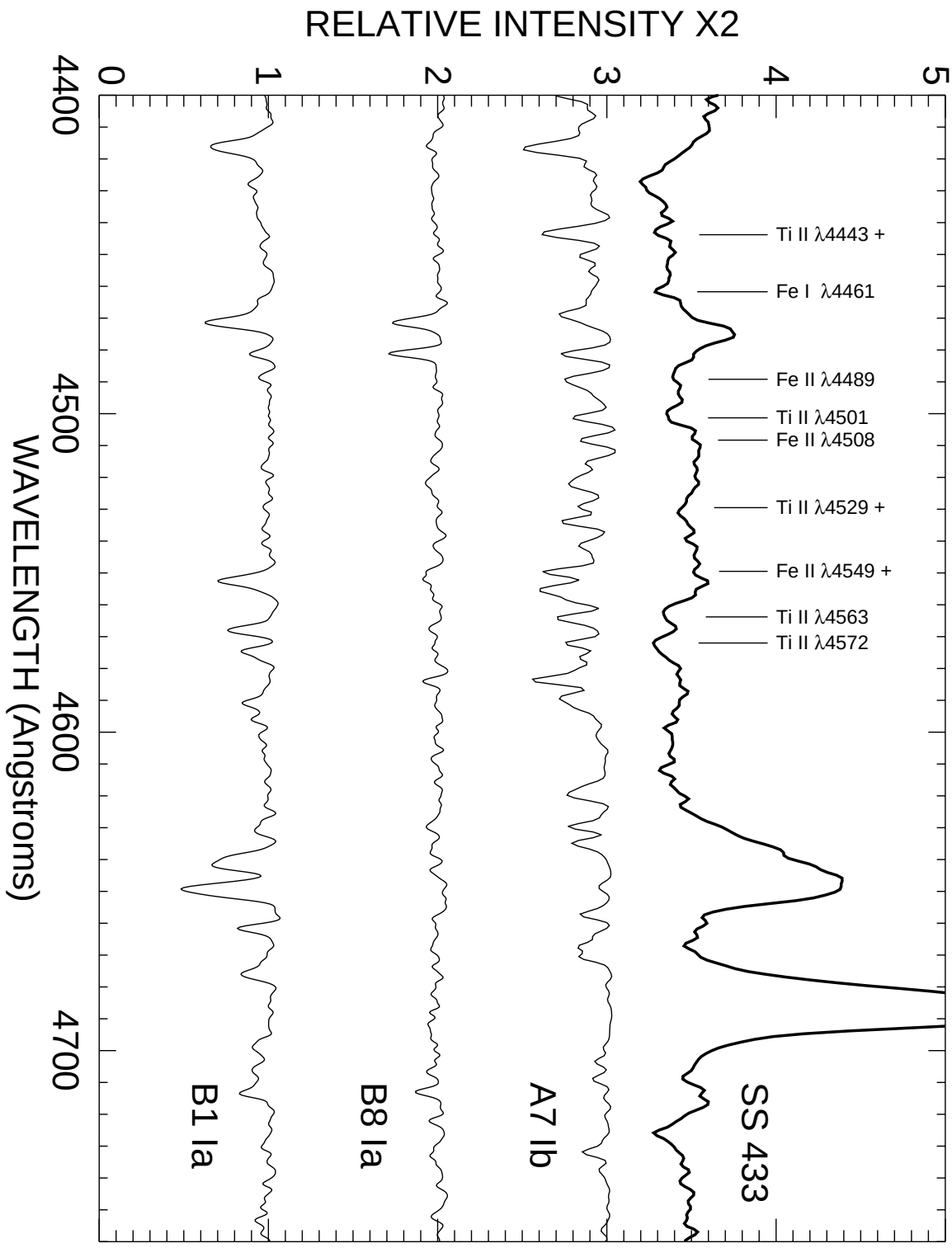
RELATIVE INTENSITY X2
0
1
2
3
4
5
4400
4500
4600
4700
WAVELENGTH (Angstroms)
B1 Ia
B8 Ia
A7 Ib
SS 433
Ti II λ4443 +
Fe I λ4461
Fe II λ4489
Ti II λ4501
Fe II λ4508
Ti II λ4529 +
Fe II λ4549 +
Ti II λ4563
Ti II λ4572

Fig. 3.—